

Enhancing diffraction-limited images using properties of the point spread function

Alex Small

*Section on Biomedical Stochastic Physics, Laboratory of Integrative and Medical Biophysics,
National Institute of Child Health and Human Development, National Institutes of Health,
Bethesda, MD 20892*

smallalex@mail.nih.gov

Ilko Ilev

*Office of Science and Engineering Laboratories, Food and Drug Administration, Rockville,
Maryland 20851*

Victor Chernomordik, Amir Gandjbakhche

*Section on Biomedical Stochastic Physics, Laboratory of Integrative and Medical Biophysics,
National Institute of Child Health and Human Development, National Institutes of Health,
Bethesda, MD 20892*

Abstract: We propose an algorithm to enhance diffraction-limited images based on pixel-to-pixel correlations introduced by the finite width of the Point Spread Function (PSF). We simulate diffraction-limited images of point sources by convolving the PSF of a diffraction-limited lens with simulated images, and enhance the blurred images with our algorithm. Our algorithm reduces the PSF width, increases the contrast, and reveals structure on a length scale half of that resolvable in the unenhanced image. Our enhanced images compare favorably with images enhanced by conventional Tikhonov regularization.

© 2006 Optical Society of America

OCIS codes: (110.0180) Microscopy; (100.2980) Image enhancement

References and links

1. M. Born, E. Wolf, and A. B. Bhatia, *Principles of optics : electromagnetic theory of propagation, interference and diffraction of light*, 7th ed. (Cambridge University Press, Cambridge [England] ; New York, 1999).
2. M. G. Gustafsson, "Surpassing the lateral resolution limit by a factor of two using structured illumination microscopy," *J Microsc* **198** (Pt 2), 82–7 (2000).
3. J. T. Frohn, H. F. Knapp, and A. Stemmer, "True optical resolution beyond the Rayleigh limit achieved by standing wave illumination," *Proc Natl Acad Sci U S A* **97**, 7232–6 (2000).
4. A. N. Boto, P. Kok, D. S. Abrams, S. L. Braunstein, C. P. Williams, and J. P. Dowling, "Quantum interferometric optical lithography: exploiting entanglement to beat the diffraction limit," *Phys. Rev. Lett.* **85**, 2733–6 (2000).
5. M. Dyba and S. W. Hell, "Focal spots of size $\lambda/2.3$ open up far-field fluorescence microscopy at 33 nm axial resolution," *Phys. Rev. Lett.* **88**, 163,901 (2002).
6. V. Westphal and S. W. Hell, "Nanoscale resolution in the focal plane of an optical microscope," *Phys. Rev. Lett.* **94**, 143,903 (2005).
7. M. K. Sundareshan, S. Bhattacharjee, R. Inampudi, and H. Y. Pang, "Image preprocessing for improving computational efficiency in implementation of restoration and superresolution algorithms," *Appl. Opt.* **41**, 7464–74 (2002).
8. C. H. Lee, H. Y. Chiang, and H. Y. Mong, "Sub-diffraction-limit imaging based on the topographic contrast of differential confocal microscopy," *Opt. Lett.* **28**, 1772–4 (2003).

9. F. Q. Chen and D. Gerion, "Fluorescent CdSe/ZnS nanocrystal-peptide conjugates for long-term, nontoxic imaging and nuclear targeting in living cells," *Nano Letters* **4**, 1827–1832 (2004).
 10. S. W. Huang, H. Y. Mong, and C. H. Lee, "Super-resolution bright-field nanometer topographic optical microscopy based on contrast," *Microsc. Res. Tech.* **65**, 180–185 (2004).
 11. C. H. Lee and J. P. Wang, "Noninterferometric differential confocal microscopy with 2-nm depth resolution," *Opt. Commun.* **135**, 233–237 (1997).
 12. J. Högbom, "Aperture synthesis with a non-regular distribution of interferometer baselines," *Astrophys. J. Suppl. Ser.* **15**, 417–426 (1974).
 13. B. G. Clark, "An Efficient Implementation of the Algorithm CLEAN" *Astron. Astrophys.* **89**, 377–378 (1980).
 14. P. C. Hansen, *Rank-deficient and discrete ill-posed problems : numerical aspects of linear inversion*, SIAM monographs on mathematical modeling and computation (SIAM, Philadelphia, 1997).
 15. P. C. Hansen, "Regularization tools Version 3.0 for Matlab 5.2," *Numerical Algorithms* **20**, 195–196 (1999).
 16. <http://www2.imm.dtu.dk/~pch/Regutools/regutools.html>.
 17. D. Uttamchandani and S. McCulloch, "Optical nanosensors - Towards the development of intracellular monitoring," *Advanced Drug Delivery Reviews* **21**, 239–247 (1996).
-

1. Introduction

Due to the fundamental Rayleigh diffraction limit, an aberration-free lens cannot clearly resolve features smaller than approximately $\lambda/(2NA)$, where λ is the wavelength of light and NA is the numerical aperture of the imaging system [1]. This limitation corresponds to the width of the point spread function (PSF). Techniques for circumventing the diffraction limit typically involve either specialized illumination [2, 3, 4, 5, 6], or enhancement of blurry images [7, 8]. Specialized illumination techniques like stimulated emission depletion (STED), when used on fluorescent samples, can achieve excellent spatial resolution ($\approx \lambda/50$) by bleaching fluorescence from the edge of the PSF. However, STED and other techniques based on illumination require more elaborate equipment than conventional optical microscopy. Superresolution algorithms, while requiring no specialized equipment, tend to be mathematically complicated [7].

We have developed an algorithm that is far simpler than most other image enhancement techniques, and can yield significant enhancement of lateral resolution in a single step. It works particularly well for the resolution of small, bright objects on dark backgrounds, conditions frequently realized with small fluorescent probes in biological samples [9]. Unlike most super-resolution algorithms, our goal is not to transform a blurry image into a collection of discrete point objects. Rather, we seek to enhance images with 3 goals: (1) Reveal the presence of multiple probes when diffraction blur makes it difficult to discern whether the image contains a single probe or multiple probes, (2) track the spacing between probes separated by a distance shorter than λ , and (3) track changes in the relative intensities of two probes separated by a distance shorter than λ . These enhancement capabilities are desirable in biology, where fluorescent probes separated by short distances may aggregate or move apart in the course of an experiment, or fluctuate in intensity in response to changes in the local environment. As we show in this paper, our algorithm achieves these goals, is competitive with other image enhancement techniques, and is exceedingly simple to implement.

Our algorithm exploits the fact that the finite width of the PSF introduces correlations between pixels. When using a microscope objective to image an object onto an array of pixels, we can think of the signal recorded by a pixel as being the sum of two distinct parts: (1) light from a conjugate region on the object; and (2) light from neighboring regions on the object, directed onto the pixel by diffraction from the finite aperture. It is the second part of the signal that introduces blur and limits image resolution. If the second part of the signal can be accurately estimated, we can correct for it and enhance an image to reveal features smaller than the diffraction limit, typically 500 nm in optical microscopy. We use the basic features of the diffraction-limited PSF (width, slope, and node) to compare a pixel with other pixels in its vicinity and estimate the contamination portion of the signal. Our technique can provide infor-

mation on the distribution of fluorescent probes down to length scales as small as 40% of the Rayleigh limit.

2. Constructing the algorithm

We will initially discuss imaging without noise, and near the end of this section discuss the effects of noise and how to deal with it. In all of this analysis we will assume that the object being imaged consists of a handful of sparse point sources, a situation realized in many biological experiments with fluorescent probes.

Consider a single light source in the focal plane of a diffraction-limited lens. If the source has a width much smaller than λ , and also smaller than dx/M , where dx is the width of a pixel in our detector and M is the magnification of our imaging system, then we can regard it as a point source. In the image plane, we will see an Airy Disk with a profile given by

$$I(r) = \left(\frac{J_1(\text{NA} \cdot k_0 \cdot r/M)}{\text{NA} \cdot k_0 \cdot r/M} \right)^2 \quad (1)$$

where r is the radial distance in the image plane, $k_0 = 2\pi/\lambda$, and J_1 is the first order Bessel function (of the first kind) [1]. The PSF is plotted as a function of distance in Fig. 1. We will focus on two key features of this PSF. The first is the node located at $r_1 = 0.61 \cdot \lambda \cdot M/\text{NA}$. For visible light ($\lambda = 400 - 700$ nm) and a decent objective ($\text{NA} = 0.5$ for convenience), this corresponds to a distance of 600 nm in the object plane. The second feature of interest is the inflection point, where the slope of the PSF is a maximum. This is located at $r_2 = 0.235 \cdot \lambda \cdot M/\text{NA}$, which for our choice of parameters corresponds to a distance of 235 nm in the image plane. These key features are indicated in the plot in Fig. 1.

Our imaging geometry is indicated in Fig. 2. Consider a pixel, which we will call P, in the image plane of a diffraction-limited lens. P is conjugate to a region of the object plane which we will call O, and receives light from O, as well as light from neighboring areas of the object plane. Our goal is to get a good estimate of the amount of light coming from sources located within the region O in the object plane.

We begin by using the node of the PSF to estimate and subtract the portion of the signal due to blur. In Fig. 2 we have drawn a ring R1 of pixels located at a distance r_1 from P (where r_1 , as above, corresponds to the first node of the PSF in Fig. 1). These pixels are not receiving any light from O. If we are trying to image fluorescent probes separated by a distance shorter than the diffraction limit, then we can assume that any light falling on these pixels is dominated by light from objects close to O, which contribute blur to the signal recorded at P. By averaging the signals recorded on the pixels located along R1 we get an estimate of the amount of blur included in the signal at P.

We can also gain information by considering the ring R2, located at a distance from P corresponding to the inflection point of the PSF ($r_2 = 0.235 \cdot \lambda \cdot M/\text{NA}$, as above). Due to the steep slope of the PSF at that distance, the signal along R2 is especially sensitive to small displacements of light sources at or near O in the object plane. This is similar to the concept exploited in differential confocal microscopy [10, 11]. If the intensity registered at the pixel P (after background subtraction) is I_1 , then if there were only a point source at O and no other light sources in the vicinity, every pixel along R2 would register a value $PSF(r_2) * I_1 = 0.56 * I_1$. However, if different pixels along R2 record different values then we can conclude that they are receiving light from sources other than whatever is located at O. The pixel recording the lowest value along R2 is the one that received the least light from sources not located at O. This is similar in spirit to the CLEAN algorithm [12, 13], in which local extrema are used to infer information on the distribution of radiation sources. However, we use minima rather than maxima, and at each step only search for minima in a small portion of the image.

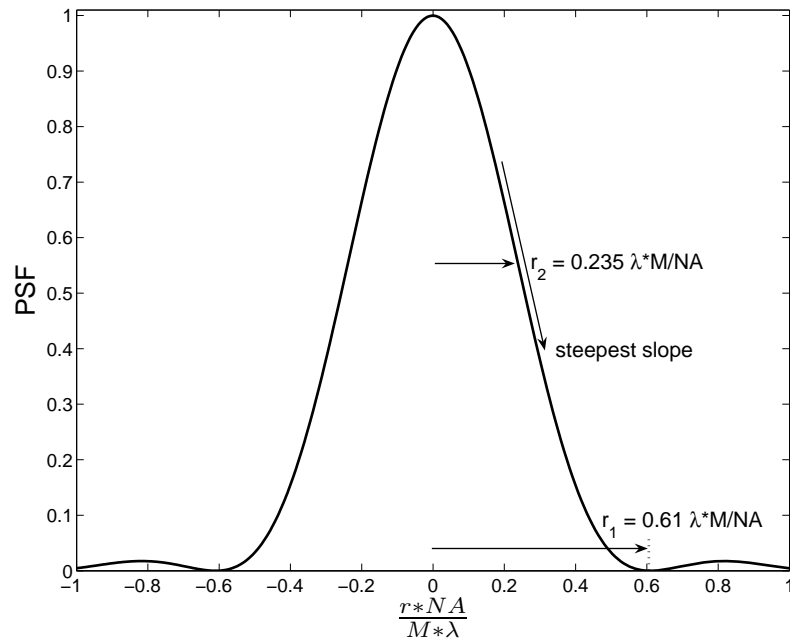


Fig. 1. A plot of the PSF for a diffraction-limited lens, identifying the node (located at r_1) and point of steepest slope (located at r_2). Both of these features are exploited by our algorithm.

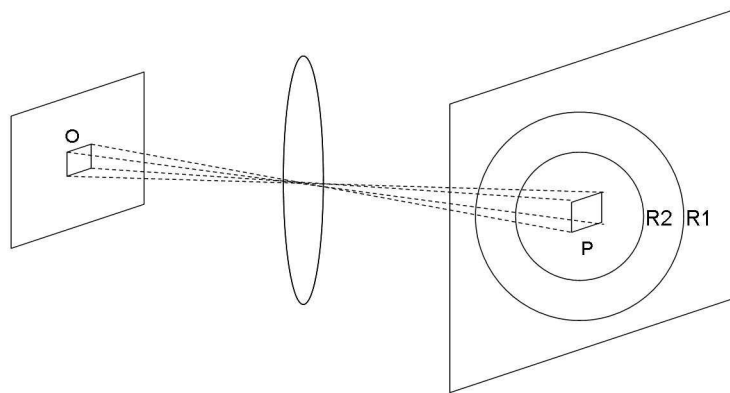


Fig. 2. An illustration of our imaging geometry. A region O in the object plane is imaged onto a pixel P in the image plane. When enhancing the image we examine pixels along the rings R1 and R2, which correspond to the node and inflection point of the PSF, respectively.

We cannot, however, conclude automatically that the pixel recording the lowest value along R2 is the one providing the best estimate of the light source located at O. We must also consider the light detected at the pixel P. If the other light sources are close to O but not symmetrically distributed around O, then they will send more light to pixel P than they send to at least some of the pixels along the circle R2, and the lowest value recorded along R2 will be less than $0.56 \cdot I_1$. In this case, we should use the lowest value recorded along R2 to estimate the light coming from O, and divide that value by 0.56 to account for the shape of the PSF. On the other hand, if the other light sources are located somewhat farther from the point O in the object plane, or evenly distributed around O, then the pixels along R2 will receive more light from those sources than the pixel P. In that case, the lowest value recorded along R2 will be greater than $0.56 \cdot I_1$, and we should simply use the value recorded at the pixel P (I_1) as the best estimate of the light coming from O.

These considerations motivate us to propose the following two-step algorithm for enhancing diffraction-limited images:

Step 1: For each pixel in the image, draw a ring R1 around it, with a radius corresponding to the first node of the PSF ($r = 0.61 \cdot \lambda \cdot M/NA$). Compute the average intensity along the edge of this circle, and subtract that average from the signal measured at the center of the circle. Set all negative values equal to zero, since negative values indicate a pixel is recording diffraction blur rather than light from a conjugate region in the object plane.

Step 2: For each pixel in the post-subtraction image, draw a ring R2 around it, with a radius corresponding to the inflection point of the PSF ($r = 0.235 \cdot \lambda \cdot M/NA$). Find the minimum intensity I_{min} along R2 and compare it with the intensity I_1 at the center of the ring. If $I_{min} < 0.56 I_1$, replace I_1 with $I_{min}/0.56$. Otherwise, leave I_1 unchanged.

Noise is an obvious concern in the second step, which selects a minimum. Anomalously low values could be propagated. However, imaging systems commonly used with microscopes can achieve noise levels lower than 1%. If noise reduction is not possible with the hardware in use, noise can be filtered with a simple moving average. The information used in step 2 comes from the linear portion of the PSF, which has a width of approximately 200 nm. A moving average taken over a box with width ≤ 200 nm can reduce noise without washing out the signal of interest, since a moving average applied to a linear function returns the same linear function.

It is also worth discussing whether the logic of the second step can be said to hold rigorously after the background subtraction in the first step. We have examined this issue, and found that properly accounting for the effects of background subtraction would require that we use a value of r_2 that is about 5% lower, and reduce the 0.56 ratio to approximately 0.52. However, the precise values of the optimal adjustments depend somewhat on the content of the image. Also, optimizing the parameters yields only slight improvements in performance (barely noticeable under visual inspection), as long as the second step is working in the linear portion of the PSF. As long as we are working in that linear region, where the slope is steep and approximately constant, the precise radius used does not matter appreciably. We see this robustness against small changes in parameters as a virtue of our algorithm.

We also note that our algorithm can be easily modified for situations in which the PSF differs from Equation (1), perhaps due to aberrations, or washing out of the nodes due to non-monochromatic illumination. In all such cases there will still be a distance at which the slope of the PSF is maximized. The second step of the algorithm can therefore be changed simply by substituting the appropriate radius and value of the PSF. The first step of the algorithm, estimating a background, can also be implemented for any realistic PSF, even if the node of the PSF is washed out. Draw the circle R1 at a distance where the PSF has decayed to a small (user-defined) value ϵ , and average the signal recorded around R1. That average signal represents the background, plus a contribution due to the object at the center, with value ϵ times the center

value. It is therefore easy to correct the background estimate before subtracting it.

3. Methods

We tested our algorithm computationally. We generated arrays of pixels bright point sources on a dark background. We then convolved these arrays with the PSF of a diffraction-limited lens, given by Equation (1), to simulate the image that a diffraction-limited lens would produce. For computational simplicity, the PSF was truncated to zero after the third node (corresponding to a distance of $1.6 \mu\text{m}$ in the object plane). Past the third node, the PSF is less than 0.2% of its maximum value, and hence negligible. Finally, we enhanced our images with the algorithm described above. All calculations were performed in Matlab.

We assumed a wavelength $\lambda = 500 \text{ nm}$, and a lens with $\text{NA} = 0.5$. We typically assumed a pixel size of $4 \mu\text{m}$, comparable to high quality digital cameras. Assuming an imaging system with a magnification of 100, $4 \mu\text{m}$ pixels in the image plane correspond to 40 nm squares in the object plane. Calculations with smaller pixel sizes ($1.25 \mu\text{m}$ or $2.5 \mu\text{m}$, corresponding to 12.5 nm or 25 nm squares in the image plane) were performed and compared with the lower-resolution results to verify that our results were in no way artifacts of pixel size. We will generally show the lower-resolution images, as they are more realistic given current hardware. However, work performed at higher resolution will also be shown, and the higher resolution will be noted.

To simulate the effects of noise in light detection, we introduced Poisson noise into the diffraction-limited images. At each pixel we generated a random number from a Poisson distribution, using the “imnoise” command in Matlab. The mean and variance of the Poisson distribution were set by the pixel value in the diffraction-limited image (before the introduction of noise). Except when noted, each image was normalized so that, prior to the introduction of noise, the peak value was 100 counts, giving a Poisson distribution with a mean of 100 and a standard deviation of 10, or a signal to noise ratio of 20 dB. This noise level was chosen to test the performance of our system under realistic conditions. Noisy images were then smoothed by a moving average with a box width of either 120 nm ($4 \mu\text{m}$ pixels) or 100 nm ($1.25 \mu\text{m}$ and $2.5 \mu\text{m}$ pixels).

4. Results

We begin with the simplest case, of a single point source. In Figure 3 we show (a) diffraction-limited and (b) enhanced images of a point source. The intensity profile (c) shows that the diffraction blur is not only narrower in the smoothed and enhanced image ($\approx 200 \text{ nm}$ vs. 500 nm full width at half maximum, or FWHM), it also has a steeper profile without a flat top, giving greater contrast.

In Fig. 4 we show diffraction-limited and enhanced images of pairs of point sources (equal intensities) separated by 400 nm and 240 nm . In one of the cases the point sources are located along a diagonal axis rather than the horizontal direction, to demonstrate that our algorithm’s results are independent of orientation. Enhancement fails to resolve the image into distinct point objects. However, it does significantly increase the aspect ratio of the image, clearly revealing the presence of structure.. We have verified that the same qualitative behavior remains for a range of pixel sizes (down to 12.5 nm in the object plane) and noise levels.

More importantly, our algorithm shrinks the horizontal FWHM of the image (and hence the estimate of the object spacing) to approximately the object spacing. This trend continues down to probe spacings as small as 200 nm ($\lambda/(2.5 \cdot \text{NA})$). By way of comparison, the diffraction-limited images over-estimate object spacings by approximately 500 nm . Looking in the vertical direction (transverse to the line connecting the point sources), diffraction-limited images only localize the sources within approximately 500 nm , while our images localize the point objects

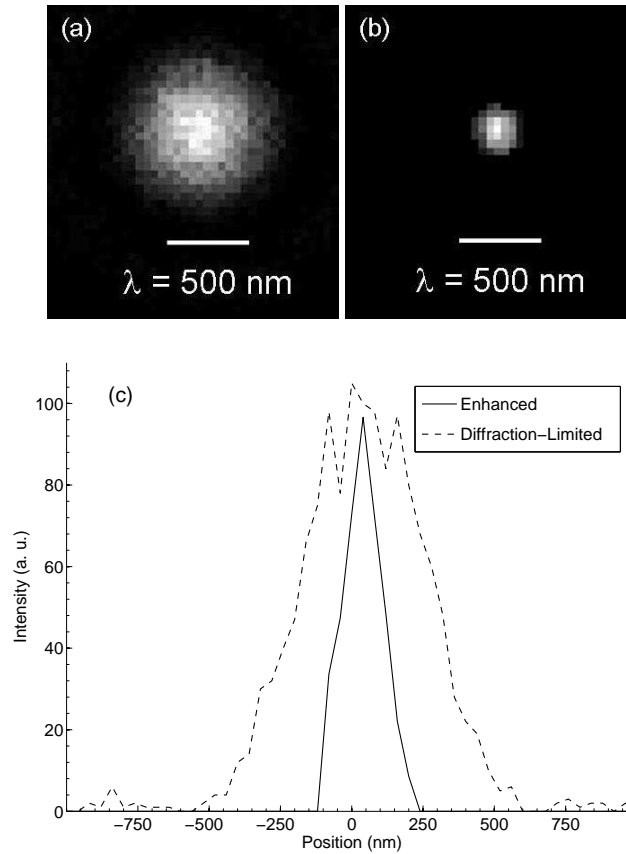


Fig. 3. (a) Diffraction-limited image of a point source. (b) Enhanced image. (Scale bars indicate wavelength of light). (c) Intensity profile of diffraction-limited and enhanced images, taken along the horizontal axis through the center of each image. Features and asymmetry due to noise and pixellation.

to a region 150-200 nm across, with the vertical localization improving as the object separation increases. If the user knows these aspects and limitations of the algorithm, quantitative information can be inferred concerning the spatial distribution of fluorophores in a microscopy experiment.

To explore the aspect ratio issue more quantitatively, in Fig. 5 we plot the aspect ratios of diffraction-limited and enhanced images as a function of object spacing. The aspect ratios were estimated from the FWHM measured along the horizontal and vertical directions. The error bars reflect the uncertainty due to finite pixel size, and so to minimize the effects of pixel size we analyzed images with smaller pixels, corresponding to 12.5 nm in the object plane. For these purposes we also refrained from introducing noise, although we have verified that moderate noise does not significantly affect aspect ratios. The difference between the diffraction-limited and enhanced images remains significant down to separations of approximately 200 nm, or $\lambda/5NA$ in terms of our computational parameters. Significantly, this corresponds to the FWHM obtained when enhancing an image of a single point source. It seems that $\lambda/5NA$, or approximately 40% of the Rayleigh limit, is the limit of resolution when applying our method to images of fluorescent point probes, consistent with the FWHM obtained for a point source

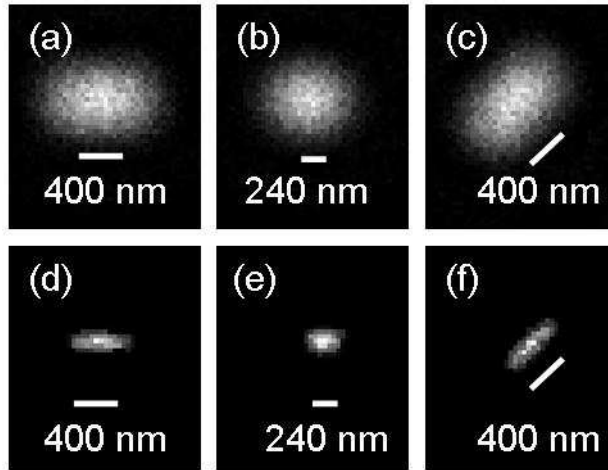


Fig. 4. Images of two point objects of equal intensity, with spacings noted on scale bars: (a), (b), (c) Diffraction-limited images; (d), (e), (f) Enhanced images.

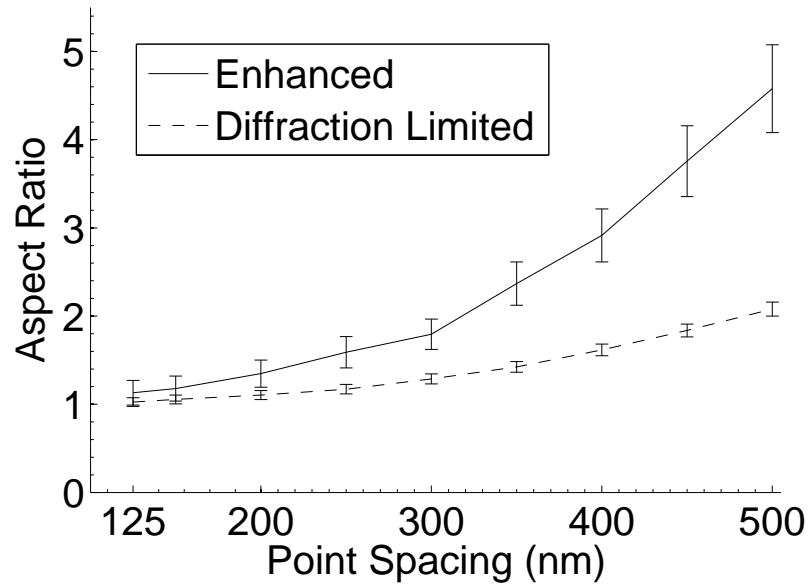


Fig. 5. Aspect ratios of diffraction-limited and enhanced images of two point objects of equal intensity, plotted as a function of the object spacing.

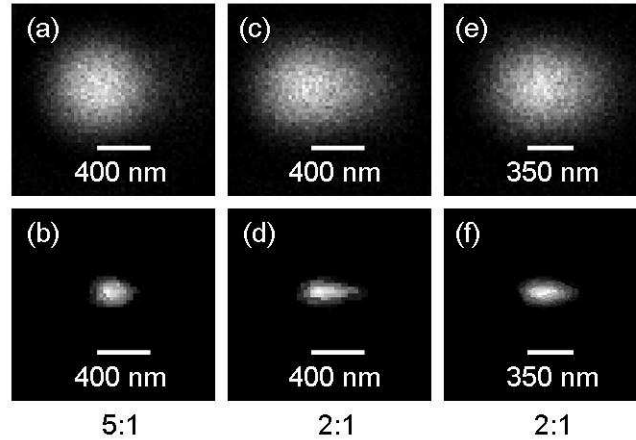


Fig. 6. Images of two point objects of unequal intensity, with spacings indicated by scale bars and intensity ratios noted below. (a),(c),(e) Diffraction-limited images. (b),(d),(f) Enhanced images.

in Fig. 3.

We also analyzed images of point sources with unequal intensities. Representative images are shown in Fig. 6. When such images are enhanced, a noticeable “tear drop” shape is revealed. The distinctive shape becomes more pronounced with increasing contrast ratio but less pronounced with decreased object spacing. Unlike aspect ratio enhancement, the tear drop shape due to contrast between the point sources is only visually apparent for object spacings greater than approximately 300 nm. To better highlight the teardrop shape, we used a pixel size of 2.5 μm on a side (25 nm in the object plane). For the noise level, we again normalized so that the peak value in each image was 100 before enhancement. Since we are using smaller pixels, this corresponds to a longer integration time.

We have also applied our algorithm to images more complicated than two discrete point objects. When working with multiple point objects, the main limitation we find is that we cannot distinguish between, say, a pair of fluorescent probes separated by 400 nm or a row of several fluorescent probes in a row spanning 400 nm. Also, it becomes very difficult to distinguish a roughly circular distribution of molecules from a single molecule, if the molecules are separated by less than approximately λ/NA . However, in the hands of a careful user this is not an insurmountable flaw. In many cell biology experiments the observer is interested in whether two molecules came together, whether molecules are inside or outside an organelle, or whether a molecule crossed a membrane[9]. In all such circumstances, it is useful to have the ability to infer the existence of multiple probes (as opposed to a single bright probe) and measure distances smaller than the diffraction limit. And frequently the experimenter will know whether the events under observation are likely to involve two probes or many probes, based on prior knowledge of his system. Also, applying our method to images more complicated than discrete and sparse point sources fails to achieve significant enhancements. However, as we have emphasized, our algorithm remains useful for situations commonly encountered in cell biology.

5. Comparison with conventional Tikhonov regularization

We compared our algorithm with enhancement by conventional Tikhonov regularization [14]. Tikhonov regularization approaches image enhancement as an inverse problem: Consider the

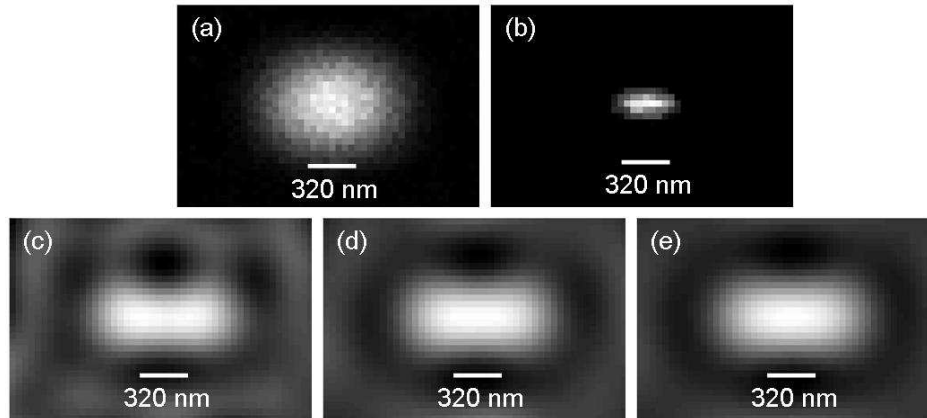


Fig. 7. Images of two point sources separated by 320 nm (scale bar). (a) Original diffraction-limited image. (b) Image enhanced by our method. (c)-(e) Images enhanced by Tikhonov regularization with regularization parameter $\lambda =$ (c) 1.0, (d) 4.3, and (e) 10.0.

PSF as a matrix acting on a vector of intensity values (pixels in the original object) to produce a new vector of intensity values (pixels in the final image). If the PSF matrix is inverted, then in principle the original image can be obtained from the diffraction-limited image. In practice, however, the inverse of the PSF matrix acts to strongly amplify noise. Some tradeoff is therefore needed between avoiding noise amplification and enhancing features. Methods that make these tradeoffs are called regularization methods, and a particularly common and easy to understand method is called Tikhonov regularization. Tikhonov regularization quantifies this tradeoff with a dimensionless parameter called λ , where $\lambda = 0$ corresponds to naive inversion of the PSF matrix, and increasing the value of λ gives greater weight to avoiding noise amplification. (Deference to two different conventions unfortunately requires that we attribute two different meanings to the same symbol, a situation for which we most heartily apologize.) For a detailed description of Tikhonov's method and methods for choosing the parameter λ see the references [14].

We implemented Tikhonov's method with the publicly available package *Regularization Tools 3.1* by P.C. Hansen [15, 16]. This package of tools can be implemented in Matlab. To avoid any complications associated with spatially correlated noise, we skipped the moving average step and instead worked at a lower noise level (maximum counts value is 300 instead of 100). This should also favor Tikhonov regularization in the comparison, since regularization becomes closer to exact deconvolution as the noise level becomes lower, while even in the absence of noise there are limits to how much information our algorithm can reveal in an image. We chose the regularization parameter $\lambda = 4.31$ by using the L curve method [16, 14]. We compared these results with a range of regularization parameters ($\lambda = 0.1$ to $\lambda = 10$).

In Fig. 7 we show (a) diffraction-limited and (b)-(e) enhanced images of two point sources separated by 320 nm. Application of the Tikhonov method in (c), (d), and (e) fails to achieve any significant improvement of the image, revealing neither distinct points nor enhancing the aspect ratio of the blur. We show images enhanced with regularization parameter $\lambda = 1, 4.31, \text{ and } 10$. The images are remarkably similar, confirming that the lack of significant improvement cannot be explained by extreme sensitivity to parameters. Tikhonov regularization provides a hint of the two-point structure of the image, but the width in the enhanced image has no correspondence to the actual probe spacing, which would be desirable in many biological experiments. Tikhonov regularization also amplifies noise, producing ringing and haloes that would tend to

obscure nearby dim objects in more elaborate images. Decreasing the regularization parameter even further amplified noise and introduced a background extending beyond the range of the blur in the original image (a). Further increases in the regularization parameter suppressed background and slightly decreased the aspect ratio of the enhanced image, the precise opposite of what we want when looking for structure. By comparison, our method significantly enhanced the aspect ratio of the diffraction blur without introducing background artifacts.

6. Conclusions

We have introduced a simple and effective method for enhancing diffraction-limited images of sparse point sources, conditions frequently realized in biological experiments with fluorescent probes. Our method can be used to qualitatively track changes in probe spacing and relative intensity. As long as the probes are separated by more than 200 nm, the aspect ratio will reveal the presence of multiple probes, and the size of the blur will approximately track the object spacing. Contrast fluctuations can be tracked by monitoring the shape of the enhanced blur. Changes in contrast may be especially interesting if the fluorescent intensity is sensitive to the local environment or concentration of a dissolved species, enabling detection of concentration gradients. Most significantly, the relative simplicity of our method compared with many super-resolution algorithms makes it ideal for enhancing movies of fluorescent probes. Work is in progress to verify the capabilities of our algorithm with real images rather than simulations. A particularly promising way to test the algorithm is with fiber-optic nanoscale probe [17]. Unlike fluorescent probes, which can diffuse, and also vary in brightness due to their environment, we can control the spacing and relative intensities of fiber-optic nanoscale probes.

Also, the efficacy of our very simple method underscores two ideas that may be fruitful for future work. The first is that the correlations introduced by diffraction have finite spatial extent. Pixels outside the range of the PSF can either be disregarded in a computation, or used to estimate a background. These ideas reinforce the significance of wavelets in image processing. The second idea is that the most important information transferred to the image plane by a diffraction-limited lens is not stored in the center of the diffraction blur. The center of the PSF is flat, and small displacements yield only small changes in the signal. Rather, the most important information is actually off-center, where the slope of the PSF is a maximum and small displacements yield large changes in intensity. This idea has previously been exploited to improve the longitudinal resolution of image acquisition in differential confocal microscopy, and now we have exploited this idea to enhance lateral resolution in a post-acquisition technique. We speculate that it may also be possible to enhance lateral resolution in image acquisition using these ideas, perhaps achieving resolution on length scales that are inaccessible to our post-acquisition approach.

Acknowledgments

We thank Jason Riley and Brian Todd for useful discussions of Tikhonov regularization, and Abby Vogel for useful feedback during the writing process. This work was supported by the Intramural Research Program of the National Institute of Child Health and Human Development, National Institutes of Health.